General Disclaimer

One or more of the Following Statements may affect this Document

- This document has been reproduced from the best copy furnished by the organizational source. It is being released in the interest of making available as much information as possible.

- This document may contain data, which exceeds the sheet parameters. It was furnished in this condition by the organizational source and is the best copy available.

- This document may contain tone-on-tone or color graphs, charts and/or pictures, which have been reproduced in black and white.

- This document is paginated as submitted by the original source.

- Portions of this document are not fully legible due to the historical nature of some of the material. However, it is the best reproduction available from the original submission.

Produced by the NASA Center for Aerospace Information (CASI)

NASA Technical Memorandum 83067

Friction and Wear of Some Ferrous-Base Metallic Glasses

MAR 1983
RECEIVED
NASA STI FACILITY
ACCESS DEPT.

Kazuhisa Miyoshi and Donald H. Buckley
Lewis Research Center
Cleveland, Ohio

(NASA-TM-83067) FRICTION AND WEAR OF SOME FERROUS-BASE METALLIC GLASSES (NASA) 24 p HC A02/MF A01 CSCL 11F
N83-19886
Unclas
G3/26 03032

Prepared for the
Joint Lubrication Conference
cosponsored by the American Society of Mechanical Engineers
and the American Society of Lubrication Engineers
Hartford, Connecticut, October 18-20, 1983

NASA

FRICTION AND WEAR OF SOME FERROUS-BASE METALLIC GLASSES

by Kazuhisa Miyoshi and Donald H. Buckley

National Aeronautics and Space Administration
Lewis Research Center
Cleveland, Ohio 44135

E-1502

ABSTRACT

Sliding friction experiments, X-ray photoelectron spectroscopy (XPS) analysis, and electron microscopy and diffraction studies were conducted with ferrous-base metallic glasses (amorphous alloys) in contact with aluminum oxide at temperatures to 750° C in a vacuum. Sliding friction experiments were also conducted in argon and air atmospheres.

The results of the investigation indicate that the coefficient of friction increases with increasing temperature to 350° C in vacuum. The increase in friction is due to an increase in adhesion resulting from surface segregation of boric oxide and/or silicon oxide to the surface of the foil. Above 500° C the coefficient of friction decreased rapidly. The decrease correlates with the segregation of boron nitride to the surface. Contaminants can come from the bulk of the material to the surface upon heating and impart boric oxide and/or silicon oxide at 350° C and boron nitride above 500° C. The segregation of contaminants is responsible for the friction behavior. The amorphous alloys have superior wear resistance to crystalline 304 stainless steel. The relative concentrations of the various constituents at the surfaces of the amorphous alloys are very different from the nominal bulk compositions.

INTRODUCTION

A host of different classes of materials are used in mechanical components where adhesion, friction, wear, and lubrication are involved. The single most significant class of these materials are the metallic alloys. As a result, considerable research has been conducted to determine the effect of various properties of metallic alloys on tribological behavior.

In 1960 it was shown that by very rapid quenching of certain alloy compositions from the melt, amorphous solid phases could be formed (ref. 1). This discovery launched a new field of research activity. There are now well over 200 alloy systems that have been identified as being capable of quenching into the amorphous state (ref. 1). These alloys are referred to as metallic glasses or amorphous alloys (refs. 2 and 3).

Amorphous alloys are currently finding increased application in the aerospace industry (ref. 4). They are used for joining internal assemblies in gas turbines. Nickel-based braze foils of the BNi class are replacing the more expensive gold-base BAu-4 for use with engine valves and many other components.

A combination of favorable mechanical and physical properties makes amorphous alloy candidates for other technological applications. For example, the combination of high permeability with high hardness makes these materials suitable for use as highly developed magnetic recording devices (e.g. video tape recorders). In most high density devices, a magnetic head

in sliding contact with a magnetic tape is used for recording and playback. Therefore, the magnetic head and tape must have good wear resistance. Amorphous alloys can also be used in foil bearings. The highly disordered structures of amorphous alloys would be resistant to radiation damage and hence, have potential for use where constant mechanical properties are required under radiation. The mechanical and physical properties of amorphous alloys are, therefore, of basic scientific interest.

Amorphous alloys have several properties that make them attractive for tribological applications. These properties include great adhesion, shear strength, impact penetration, corrosion resistance, toughness, and ductility. There has been, however, relatively little research done on the tribological properties of the amorphous alloys (refs. 5 to 7).

The objective of this investigation was, therefore, to determine the surface chemistry, microstructure, and tribological properties (friction and wear) of some ferrous base amorphous alloys. Sliding friction experiments were conducted with three ferrous-base amorphous alloy compositions in vacuum (3x10 nPa), laboratory air, and argon atmosphere. A rider of aluminum oxide was made to slide on the amorphous alloy surfaces under loads of from 0.1 to 2.5 N and at sliding velocities of from 0.033 to 0.17 mm/sec. The vacuum experiments were conducted at temperatures of from 25° to 800° C. Comparative experiments were made with 304 stainless steel. This practical material was of equivalent foil thickness as the amorphous alloys.

MATERIALS

Three amorphous alloy compositions were examined in this investigation. The compositions and some of their properties are presented in table I. The alloys were foils (0.030 to 0.033 mm-thick ribbon), and were used in the as-cast condition except for heat treatments. The spherical riders that were made to slide on the foil were single-crystal aluminum oxide (sapphire) spheres and the diameter of the spheres were 3.2 and 6.4 millimeters.

APPARATUSES

Two apparatuses were used in this investigation (fig. 1). They both use a pin on flat configuration. One consists of an ultra-high vacuum system capable of measuring adhesion, load, and friction and contains an XPS spectrometer. Figure 1(a) indicates the major components, including the electron energy analyzer, the X-ray source, and the ion gun used for ion sputter etching. The X-ray source contained a magnesium anode. A manipulator-mounted beam was projected into a vacuum chamber. The beam contained two flats machined normal to each other with strain gages mounted thereon. The load was applied by moving the beam normal to the flat and was sensed by strain gages. The vertical sliding motion of the pin along the flat surface was accomplished through a motorized manipulator assembly. The friction force under an applied load was measured during vertical translation by a strain gage mounted normal to that used to measure load.

The second apparatus used in this investigation is shown schematically in figure 1(b). The pin was made to traverse a distance of 10 mm on the surface of the foil. Motion was reciprocal. The pin was loaded against the foil with dead weights. The arm retaining the rider contained strain gages to measure the tangential and normal forces. The entire apparatus was housed in a plastic box. The atmosphere in the box was controlled.

EXPERIMENTAL PROCEDURE

Specimen Preparation and Heating

The foil specimen was attached to an insulator flat with tantalum supporting sheets (fig. 1). The specimen was directly in contact with the sheets. The flat and pin surfaces were rinsed with 200-proof ethyl alcohol just before they were placed in the vacuum chamber. After the specimens were placed in the vacuum chamber, the system was evacuated and then baked out at 250° C to obtain a pressure of 3x10 nPa ($2x10^{-10}$ torr) or lower.

Both flat and pin specimens were argon ion sputter cleaned. Treatment was next conducted in situ, and this included heating to a maximum temperature of 750° C at a pressure of 3x10 nPa for 20 min to 30 min. The foil was resistance heated. The temperature was measured with a type K (Ni-Cr vs. Ni-Al) thermocouple in contact with the specimen.

Chemical Analysis of Surface

The foil surfaces were analyzed by X-ray photoelectron spectroscopy (XPS). The depth analysis with XPS is of the order of 2 to 3 nm, and the ultimate sensitivity is sufficient to allow fractions of a monolayer to be detected and identified. A magnesium K_α X-ray source was used with an X-ray source power of 400 W. All XPS analyses were conducted at room temperataure.

Friction Experiments

In the ultra-high-vacuum system, in situ friction experiments were conducted with the surface-treated foil specimens over a temperature range of from room to 750° C. A load of 0.2 N was applied to the pin-flat contact by deflecting the beam, as shown in figure 1. To obtain consistent experimental conditions, contact before sliding was maintained for 30 sec. Both the load and friction force were continuously monitored during a friction experiment. Sliding velocity was 3 mm/min with a total sliding distance of 2 to 3 mm. All single-pass friction experiments were conducted in a 3x10 nPa vacuum. The coefficients of friction reported herein were obtained by averaging three to five measurements. In argon or a laboratory air atmosphere the foils of the amorphous alloys and the pin specimen surfaces were scrubbed with levigated alumina, rinsed with tap water and then with distilled water, and finally rinsed with ethyl alcohol. After the surface was dried with argon gas, the specimens were placed into the experimental apparatus. The specimen surfaces were then brought into contact and loaded, and the friction experiment was begun.

RESULTS AND DISCUSSION

Surface Chemistry

<u>$Fe_{67}Co_{18}B_{14}Si_1$ alloy</u>. - The XPS spectra of the Fe_{2p}, Co_{2p}, B_{1s} and Si_{2p} obtained from narrow scans on the $Fe_{67}Co_{18}B_{14}Si_1$ foil surface are presented in figure 2. The as-received foil after bakeout was argon ion bombarded and then heated at various temperatures in a 3x10 nPa vacuum. All

the XPS spectra taken at room temperature revealed carbon and oxygen peaks in addition to iron, cobalt, boron and silicon.

The Fe_{2p} photoelectron peaks of the as-received specimen clearly indicate that there were iron oxides on the foil surface (ref. 8). The spectra taken after the foil surface had been argon sputter cleaned for 30 min and 60 min clearly indicated the Fe_{2p} peaks associated with iron, and these typical peaks are shown in figure 2. The spectra for the foils heated to 350° and 750° C are almost the same as that for the argon-sputter-cleaned surface.

The Co_{2p} photoelectron peaks of the as-received specimen indicate cobalt oxide at 780 eV. The spectra for the surfaces that had been argon sputter cleaned and heated to 350° and 750° C reveal cobalt and its alloy peaks. The cobalt oxide peak is negligible.

The B_{1s} photoelectron peaks of the as-received specimen indicate the presence of boric oxide as well as Fe_2B, CoB, and B. The spectrum of the surface that had been argon sputter cleaned for 30 min and 60 min reveals large peaks for boron and its alloys as well as very small boric oxide peaks. The spectra for the foils that had been heated to 350° and 750° C clearly indicate that the foil surfaces were again contaminated with boric oxide and boron nitride that had migrated from the bulk of the foil specimens.

Contaminants such as oxygen, nitrogen, and carbon may be introduced from the environment to the bulk of an amorphous alloy during the direct casting process. To refine the metallic atomic structure, an amorphous alloy must be cast at speeds to a few thousand meters per minute and at frequency rates as high as a million degrees centigrade per second.

The Si_{2p} photoelectron peaks of the as-received surface reveal silicides. Even the spectrum of the surface that had been argon sputter cleaned for 30 min and 60 min reveals silicides as well as silicon oxide on the surface. The foils that had been heated to 350° and 750° C were contaminated with silicon oxide that had migrated from the bulk of the foil specimens.

Photoelectron lines for the C_{1s} of the foil showed that an adsorbed carbon contaminant peak was evident in the spectrum for the as-received specimen. Generally, the surface of the argon ion sputter cleaned foil for 30 min contained carbon contamination as well as carbides such as silicon carbide. The spectra of the surface that had been sputter cleaned for 60 min and with the surface heated to 350° and 750° C indicated a small carbide peak. Although the $Fe_{67}Co_{18}B_{14}Si_1$ foil was not supposed to include carbon, carbides were present in the foil.

The composition of the surficial layer of the foil analyzed by XPS is summarized in table II. Generally, the XPS results indicate that surfaces that had been cleaned by argon ion sputtering or heated to 350° or 750° C consisted of iron, cobalt, boron, silicon, carbon and oxygen. The relative concentrations of the constituents on the surface were very different from the nominal bulk compositions. The surface contained less boron and more silicon, carbon, and oxygen than the bulk.

<u>$Fe_{81}B_{13.5}Si_{3.5}C_2$ and $Fe_{40}Ni_{38}Mo_4B_{18}$ alloys</u>. - Generally, the surfaces of the as-received, argon ion sputter cleaned, and heated $Fe_{81}B_{13.5}Si_{3.5}C_2$ and $Fe_{40}Ni_{38}Mo_4B_{18}$ foils contained carbon and oxygen in addition to the various alloying constituents of the nominal bulk composition. The surface conditions of these foils were basically the same as that for $Fe_{67}Co_{18}B_{14}Si_1$. The argon ion sputter cleaned surface conditions of the three

different foils analysed by XPS are summarized in table III. The relative concentrations of the various constituents were very different from the nominal compositions. The surfaces contained less boron and more silicon, carbon, and oxygen than the bulk.

Table IV summarizes the surface conditions of the foils analysed by XPS. Generally, the XPS results indicate that the surfaces of the as-received foils consisted of a layer of oxides of alloying elements as well as a simple, adsorbed film of oxygen and carbon. The argon sputter cleaned surface consisted of the alloy and small amounts of oxides and carbides. In addition to nominal element constituents, the surface heated to 350° C contained boric and silicon oxides on $Fe_{67}Co_{18}B_{14}Si_1$ and $Fe_{81}B_{13.5}Si_{3.5}C_2$ alloys, and boric oxides on $Fe_{81}Ni_{38}Mo_4B_{18}$ alloys as well as small amounts of carbides. The surface heated to 750° C contained boron nitride that had migrated from the bulk of the foil specimens, as well as small amounts of oxides.

Microstructure

To establish the exact crystalline state of the foils examined by XPS as previously described, grain boundary structures were examined by transmission electron microscopy and diffraction in a microscope operating at 100 kV. Final thinning of the foils was accomplished by electropolishing. These analysis were done after the friction experiments.

A typical example of the structure of the as-received amorphous foil is shown in figure 3. No dislocations and grain boundaries are evident in figure 3. However, black spots, which are believed to be crystallites with a size range from 1.5 to 4 nm, are apparent in the micrograph. The transmission electron diffraction pattern for the as-received foil is also presented in figure 3. The pattern indicates that the amorphous foil was not completely amorphous, but contained extremely small grains of approximately a few nanometers in size.

Typical examples of the crystallized structure of the foil heated to 500° and 750° C are shown in figures 4 and 5. The foil was subjected to heat treatment above the crystallization temperature in a vacuum of 3x10 nPa. Complete crystallization occurred after heating to 500° C. The crystallized grain size was about 0.12 to 0.70 μm. At a higher crystallization temperature of 750° C, the crystallized grain size was 0.3 to 1.4 μm.

A typical microstructure of the foils that had been heated to 500° and 750° C contained two kinds of grains: a dark grain, and a light grain. Single-crystal diffraction patterns were obtained from the dark grain as well as from the light grain after annealing at 750° C, as shown in figure 5. The grains in the foil that had been annealed at 500° C were too small to yield a diffraction pattern. Single-crystal patterns taken from both the dark and light grains included diffraction spots and Kikuchi lines.

Energy-dispersive X-ray analysis was conducted on both light and dark grains. Figure 6 presents a typical energy-dispersive X-ray profile of the light and dark grains shown in figure 5. The profile taken from the dark grain shows iron, cobalt, and copper peaks but a negligible silicon peak. The copper peaks in the spectrum are assosciated with the specimen mesh-holder. On the other hand, the spectrum taken from the light grain clearly shows a silicon peak as well as iron, cobalt, and copper peaks. Thus, the segregation of silicon occurs in amorphous alloys when they are heated to

the recrystallization temperature. No information can be obtained for boron by energy-dispersive X-ray analysis.

Quantitative analysis was done by using X-ray profiles, as shown in figure 6. The relative concentrations of the cobalt and silicon to iron are shown in table V. Table V indicates that the light grains contained about twenty times more silicon than the dark grains.

Adhesion and Friction in Vacuum

Sliding friction experiments were conducted with aluminum oxide in contact with amorphous alloys in vacuum. Friction-force traces resulting from such sliding were generally characterized by fluctuating behavior with evidence of stick-slip (ref. 7). The coefficient of friction as a function of the sliding temperature of the foil specimen is indicated in figure 7. The aluminum oxide rider was sputter cleaned with argon ions at room temperature. The foil specimen was also sputter cleaned with argon ions in the vacuum system and then heated from room temperature to 750° C. The coefficient of friction increased with increasing temperature from room to 350° C. The increase in friction is due to an increase in the adhesion resulting from segregation of boric oxides and silicon oxides to the foil surface as described earlier. Generally, the presence of oxygen does strengthen the metal-ceramic material (such as Al_2O_3, Mn-Zn and Ni-Zn ferrite, and SiC) contacts and increase the friction (refs. 9 to 11).

Above 500° C the coefficient of friction decreased dramatically. The rapid decrease in friction above 500° C correlated with the segregtion of boron nitride on the foil surface, as already discussed and shown in figure 2(c). It is also interesting in figure 7 that there is a considerable difference in the friction measured for the variations in alloy chemistry.

Friction and Wear in Argon and Air

Sliding friction experiments were conducted in argon and in air with normal residual surface oxides present on the $Fe_{67}Co_{18}B_{14}Si_1$. To compare the friction and wear characteristics to conventionally used alloys, friction experiments were conducted with 304 stainless steel foils under conditions identical to those with the amorphous alloy.

When the amorphous alloy and 304 stainless steel slid against aluminum oxide spherical pin (6.4-mm-dia.) at a load of 2.5 N for 30 min, very little difference in the friction behavior resulted between the two alloys. The coefficient of friction for both alloys was approximately 0.2 The wear results were, however, markedly different. There was a complete absence of any visible wear track on the amorphous alloy foil, but a wear track was visible on the 304 stainless steel foil. No detectable wear on the surface of the amorphous alloy was found by optical and scanning electron microscopic examinations. Considerable wear, however, to the 304 stainless steel surface was indicated by the scanning electron micrograph in figure 8. Considerable plastic flow occurred, and a copious amount of wear debris was generated on the 304 stainless steel, and clumps of metal appeared in the wear track. The surface oxide layers present on the amorphous alloy, which were discussed previously, provide a protective film against wear. The amorphous alloys have, therefore, superior wear resistance to the crystalline stainless steel alloy.

Variations in mechanical parameters such as sliding velocity and normal load do not appear to exert an effect on the friction behavior of the amorphous alloy over the range of normal loads from 0.05 N to 2.5 N and at sliding velocities of from 0.03 to 1.6 mm/sec. There was essentially no change in the coefficient of friction.

Since no visible wear was observed on the amorphous alloy, sliding friction experiments were conducted with a smaller spherical pin (3.2-mm-dia.), to provide a high contact pressure with sliding time extended to 5 hours to provide more severe experimental conditions.

With 3.2 millimeter diameter aluminum oxide pin, there were marked differences not only in friction, but also in wear behavior.

Friction was initially low, but increased with increasing sliding time, as indicated in the data of figure 9. After some period of time, an equalibrium condition was reached with the amorphous alloy and the 304 stainless steel, and then the friction did not change with sliding time.

The coefficients of friction obtained with $Fe_{67}Co_{18}B_{14}Si_1$ alloy shown in figure 9 were generally the same as those obtained from experiments conducted with 6.4 millimeter diameter aluminum oxide pin in contact with the alloy. The friction results with the 304 stainless steel are, however, markedly different when examined with 3.2 millimeter diameter aluminum oxide pin. The coefficient of friction at an equilibrium condition was nearly three times that with 6.4 millimeter diameter aluminum oxide pin.

Figure 10 presents scanning electron micrographs of typical wear tracks of the amorphous alloy and the 304 stainless steel. The experiments were conducted at a load of 2.5 newtons with a 3.2 millimeter diameter aluminum oxide pin and at a total sliding time of 5 hours. Oxide wear debris particles were generated on the amorphous alloy surface, while metal wear debris particles were primarily generated on the 304 stainless steel surface. With the amorphous alloy microscopic brittle fracture and breaking up of oxide layers took place, and fine oxide wear debris particles were mainly produced.

Figure 11 illustrates a detailed examination of the oxide wear debris (submicrons to microns in size) produced on the amorphous alloy as a result of sliding of the 3.2 millimeter diameter aluminum oxide pin for a distance of 27 m. The scanning electron micrographs clearly reveal powdery and whiskery oxide wear debris particles on and near the wear track after sliding contact with the aluminum oxide pin.

Figure 12 presents scanning electron micrographs taken in the wear track on the 304 stainless steel surface. Adhesion of aluminum oxide to stainless steel occurs across the interface. With tangential motion, separation takes place in the 304 stainless steel and rupturing the bonds of cohesively weaker 304 stainless steel occurs. And then cavities form in the material, as shown in figure 12(a). Small platelet-type metallic wear debris particles are subsequently produced, as shown in figure 12(b).

CONCLUSIONS

The following conclusions are drawn from the presented data:

1. The coefficient of friction increases with increasing temperature to 350° C in vacuum. The increase in friction is due to an increase in adhesion resulting from surface segregation of boric oxide and/or silicon oxide to the surface of the foil.

Above 500° C the coefficient of friction decreased rapidly. The decrease correlates with the segregation of boron nitride to the surface.

Contaminants can come from the bulk of the material to the surface upon heating and impart to the surface boric oxide and/or silicon oxide at 350° C and boron nitride above 500° C. The segregation of contaminants is responsible for the friction behavior.

2. The amorphous alloys have superior wear resistance to the crystalline 304 stainless steel.

3. The relative concentrations of the various constituents at the surfaces of the amorphous alloys are very different from the nominal bulk compositions.

4. It is indicative that the amorphous alloys are not completely amorphous, but contain extremely small crystallites of approximately a few nanometers (1.5 to 4 nm) in size.

5. The microstructure of crystallized amorphous alloy contains dark and light single-crystal grains as revealed by transmission electron microscopy. The dark grains contain considerably less silicon than do the light grains.

REFERENCES

1. Jones, H., "Splat Cooling and Metastable Phases," Rep. Prog. Phys., 36, 1425-1497 (1973).
2. Gilman, J. J., "Metallic Glasses," Phys. Today, 28, (5), 46-53 (1975).
3. Gilman, J. J., "Metallic Glasses - A New Technology," Crystal Growth and Materials, ed. by E. Kaldis and H. J. Scheel, Current Topics in Materials Science, vol. 1, Elsevier-North Holland Publishing Co., 1977, pp. 727-741.
4. DeCristofaro, N., and Henschel, C., "Matglas Brazing Foil," Weld. J., 57, (7), 33-38 (1978).
5. Amuzu, J. K. A., "Sliding Friction of Some Metallic Glasses," J. Phys. D., 13, (7), L127-L129 (1980).
6. Miyoshi, K., and Buckely, D. H., "Friction and Surface Chemistry of Some Ferrous-Base Metallic Glasses," NASA TP-1991, 1982.
7. Miyoshi, K., and Buckley, D. H., "Surface Chemistry, Microstructure, and Friction Properties of Some Ferrous-Base Metallic Glasses at Temperatures to 750° C," NASA TP-2006, Apr., 1982.
8. Wagner, C. D., W. M. Riggs, L. E. Davis and J. F. Moulder, G. E. Muilenberg, Handbook of X-ray Photoelectron Spectroscopy, Perkin-Elmer Corp., Physical Electronics Div., Eden Prairie, Minn. (1978).
9. Pepper, S. V., "Effect of Interfacial Species on Shear Strength of Metal-Sapphire Contact," J. Appl. Phys., 50, (12), 8062-8065 (1979).
10. Miyoshi, K. and Buckley, D. H., "The Effect of Oxygen and Nitrogen Interactions on Friction of Single-Crystal Silicon Carbide," NASA TP-1265, 1978.
11. Miyoshi, Kazuhisa; and Buckley, Donald H.: XPS and Friction Studies of Ni-Zn and Mn-Zn Ferrites in Contact with Metals. NASA TP in process.

TABLE I. - PROPERTIES OF AMORPHOUS ALLOYS

Alloy composition	Crystallization temperature, °C	Density, g/cm^3	Hardness, GPa	Ultimate tensile strength,	Bend ductility,[a] ε
$Fe_{67}Co_{18}B_{14}Si_1$	430	7.56	10	1.5	1
$Fe_{81}B_{13.5}Si_{3.5}C_2$	450	7.3	10.3	.7	9×10^{-3}
$Fe_{40}Ni_{38}Mo_4B_{18}$	410	8.02	10.5	1.38	1

[a]$\varepsilon = t/(d-t)$, where t is ribbon thickness and d is micrometer spacing at bend fracture.

TABLE II. - COMPOSITION OF AMORPHOUS ALLOY SURFICIAL LAYER

[Nominal bulk composition,[a] wt percent: $Fe_{67}Co_{18}B_{14}Si_1$; nominal bulk composition, at. percent: $Fe_{42}Co_{11}B_{46}Si_1$.]

Treatment	Composition on surface, at. percent
Argon ion sputtering	$Fe_{49}Co_{14}B_{17}Si_6C_9O_5$
Heating to 350° C	$Fe_{52}Co_{11}B_{18}Si_6C_8O_5$
Heating to 750° C	$Fe_{54}Co_9B_{19}Si_5C_8O_5$

[a]Manufacturer's analysis.

TABLE III. - COMPOSITION ON ARGON-SPUTTER-CLEANED SURFACE LAYER OF AMORPHOUS ALLOY

Nominal bulk composition		Composition on surface, at. percent
wt percent[a]	at. percent	
$Fe_{67}Co_{18}B_{14}Si_1$	$Fe_{42}Co_{11}B_{46}Si_1$	$Fe_{49}Co_{14}B_{17}Si_6C_9O_5$
$Fe_{81}B_{13.5}Si_{3.5}C_2$	$Fe_{48}B_{42}Si_4C_6$	$Fe_{43}B_{15}Si_8C_{21}O_{14}$
$Fe_{40}Ni_{38}Mo_4B_{18}$	$Fe_{23}Ni_{21}mo_1B_{55}$	$Fe_{18}Ni_{28}Mo_1B_{24}C_{15}O_{14}$

[a]Manufacturer's analysis.

TABLE IV. - SURFACE OF AMORPHOUS ALLOYS

Alloy composition	Surface			
	As received	Argon sputter cleaned	Heated to 350° C	Heated to 750° C
$Fe_{67}Co_{18}B_{14}Si_1$	Oxides of Fe, Co, B, Si, and C Adsorbed film of oxygen and carbon	Alloy Small amount of oxides and carbides	Alloy Boric oxides and silicon oxides migrated from bulk Small amount of carbides	Alloy Boron nitride migrated from bulk. Very small amount of boric oxides and silicon oxides
$Fe_{81}B_{13.5}Si_{3.5}C_2$	Oxides of Fe, B, Si, and C Adsorbed film of oxygen and carbon	Alloy Small amount of oxides and carbides	Alloy Boric oxides and silicon oxide migrated from bulk Small amount of carbides	Alloy Boron nitride migrated from bulk Very small amount of boric oxides and silicon oxides
$Fe_{40}Ni_{38}Mo_4B_{18}$	Oxides of Fe, B, Ni, Mo, and B Adsorbed film of oxygen and carbon	Alloy Small amount of oxides and carbides	Alloy Boric oxides migrated from bulk Small amount of carbides	Alloy Boron nitride migrated from bulk Very small amount of boric oxides

TABLE V. - SOLUTE-IRON CONCENTRATION RATIO OF BULK OF AN AMORPHOUS ALLOY HEATED TO 500° OR 750° C IN VACUUM (10 nPa)

(a) Heated to 500° C

Structure			
Constituent	Dark grain	Light grain	Mixed area
	Solute-iron concentration ratio		
Fe	1	1	1
Co	.3	.44	.36
Si	.001	.02	.008

(b) Heated to 750° C

Fe	1	1	1
Co	.32	.44	.37
Si	.001	.02	.008

ORIGINAL PAGE IS
OF POOR QUALITY

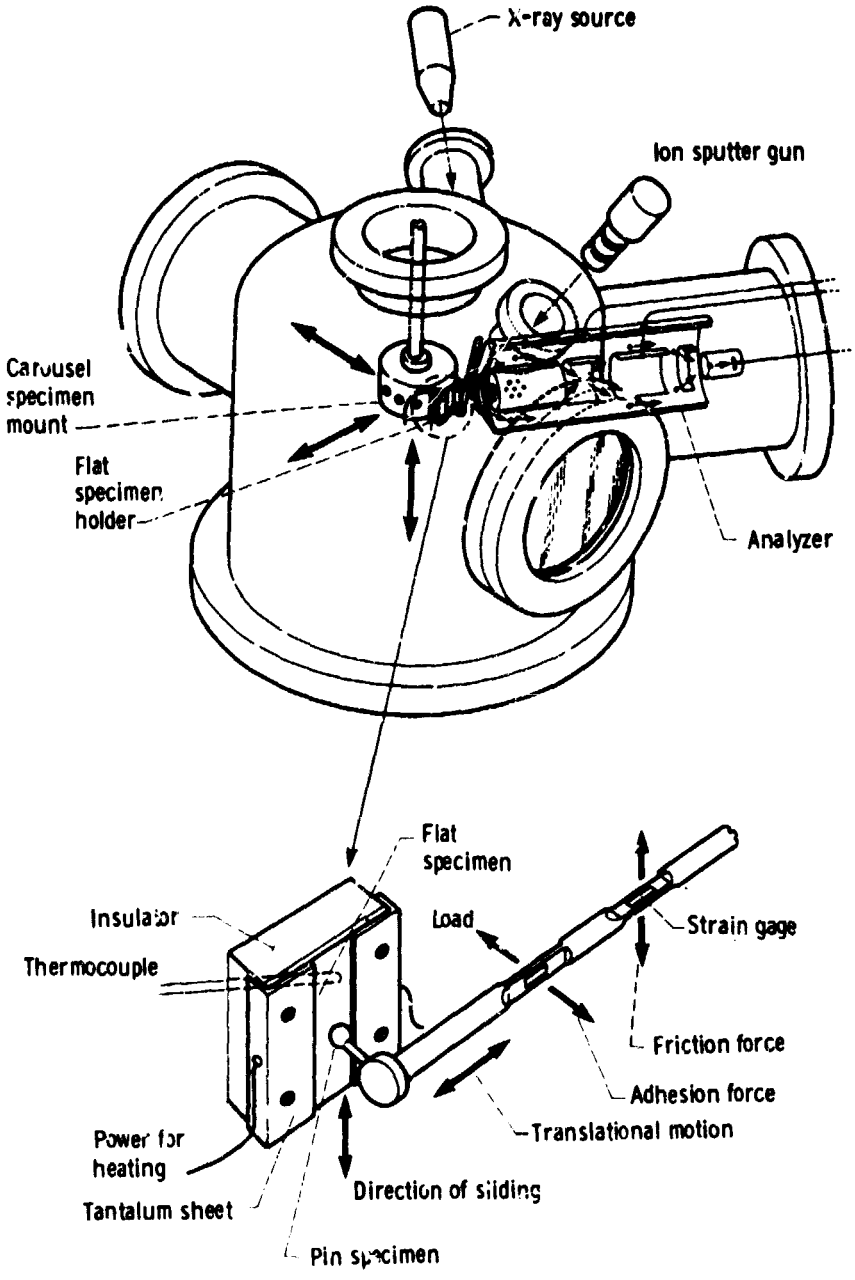

(a) Ultra high-vacuum friction and wear apparatus.

Figure 1. - Friction and wear apparatuses.

ORIGINAL PAGE IS
OF POOR QUALITY

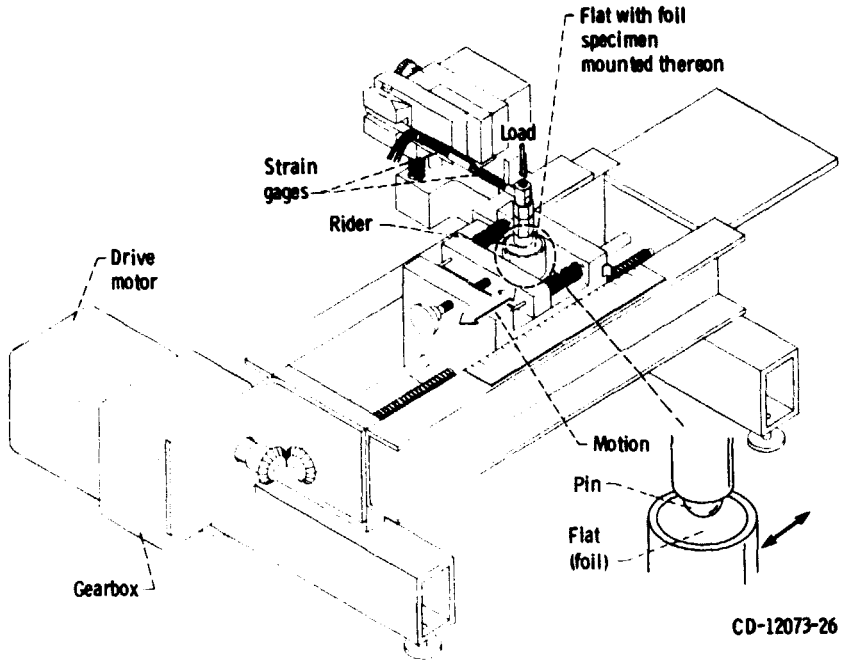

(b) Friction and wear apparatus used in argon and in laboratory air.

Figure 1. - Concluded.

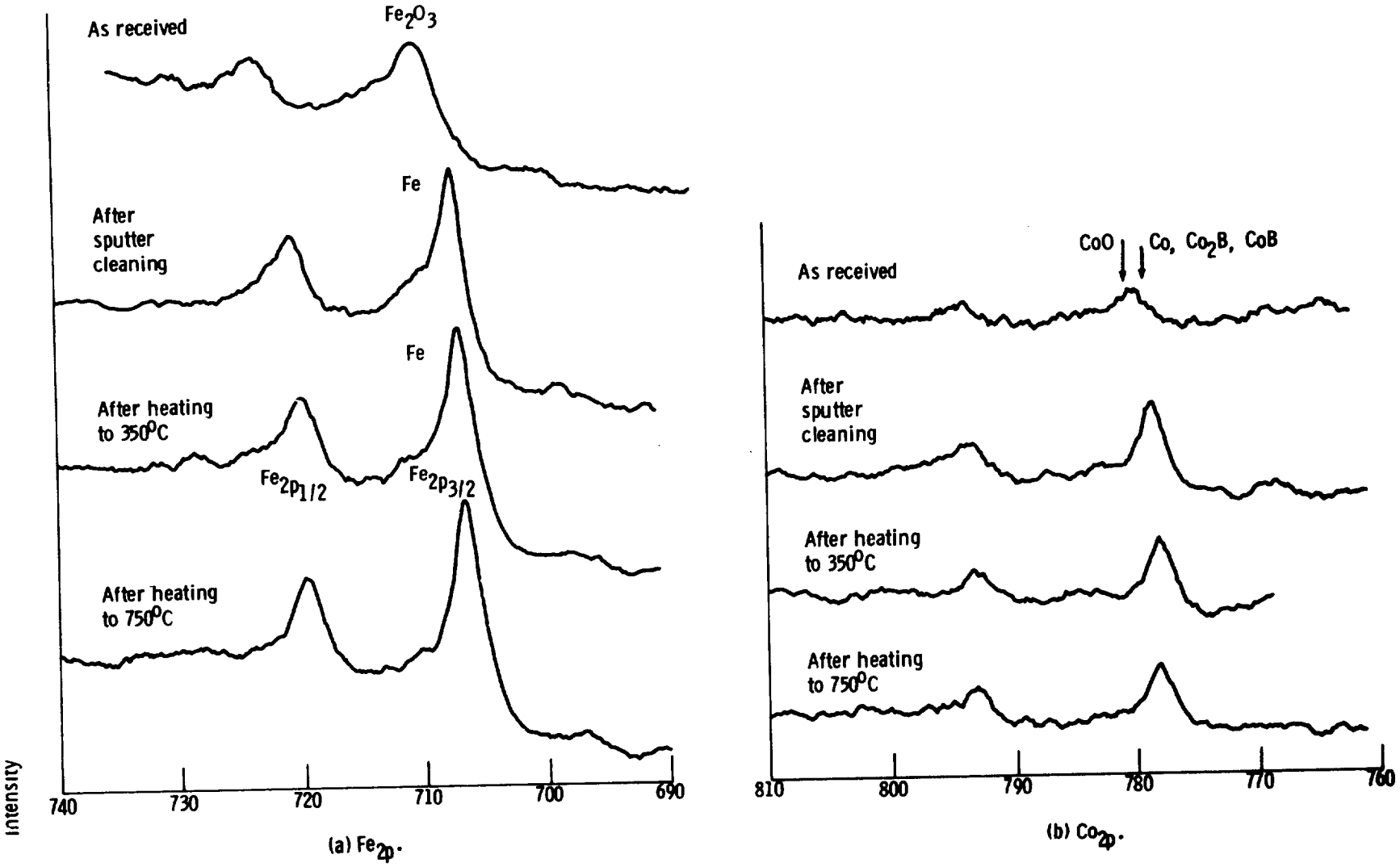

Figure 2. - Representative Fe_{2p}, Co_{2p}, B_{1s}, Si_{2p}, and C_{1s} XPS peaks on $Fe_{67}Co_{18}B_{14}Si_1$ surface.

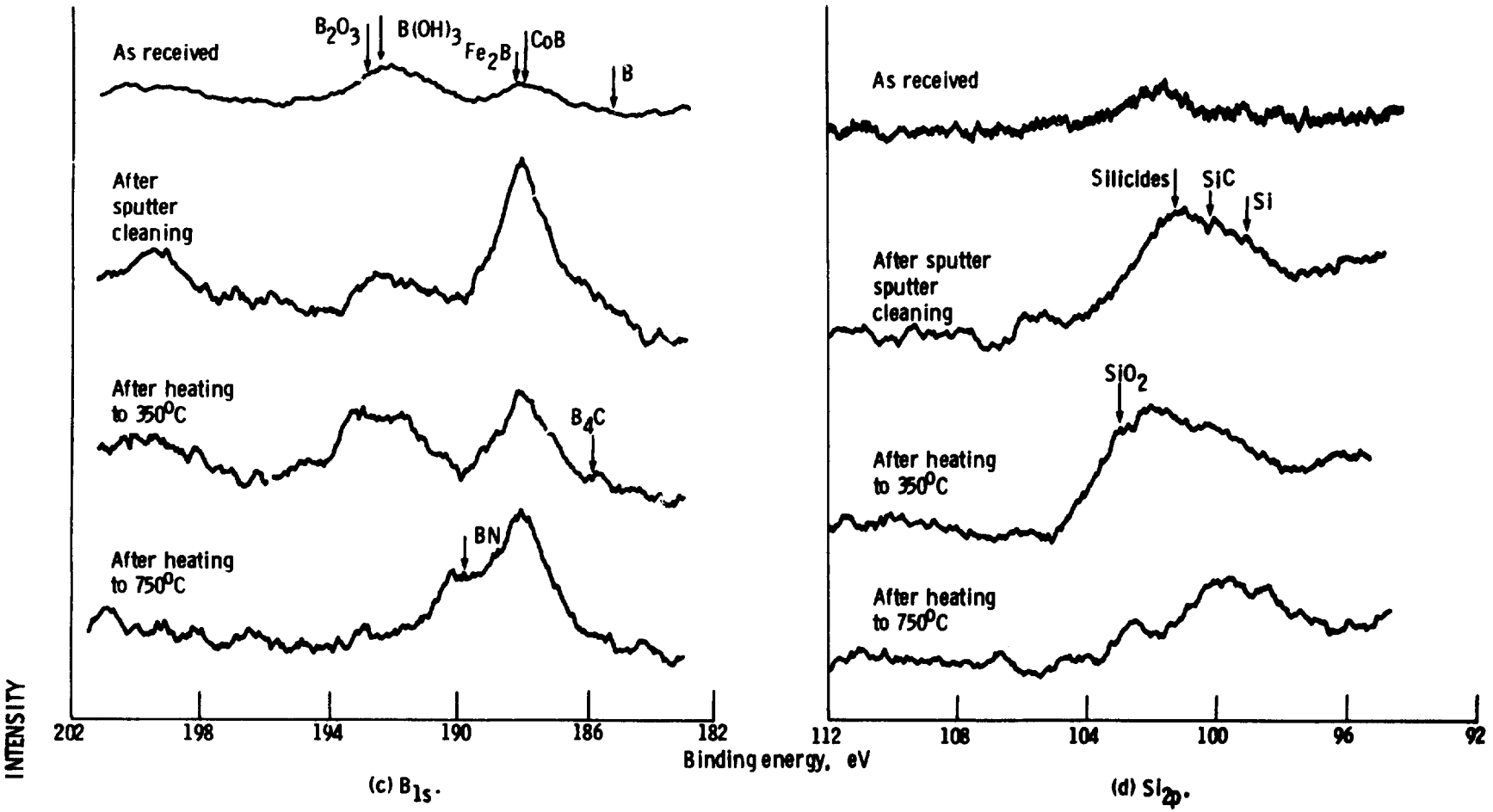

Figure 2. - Concluded.

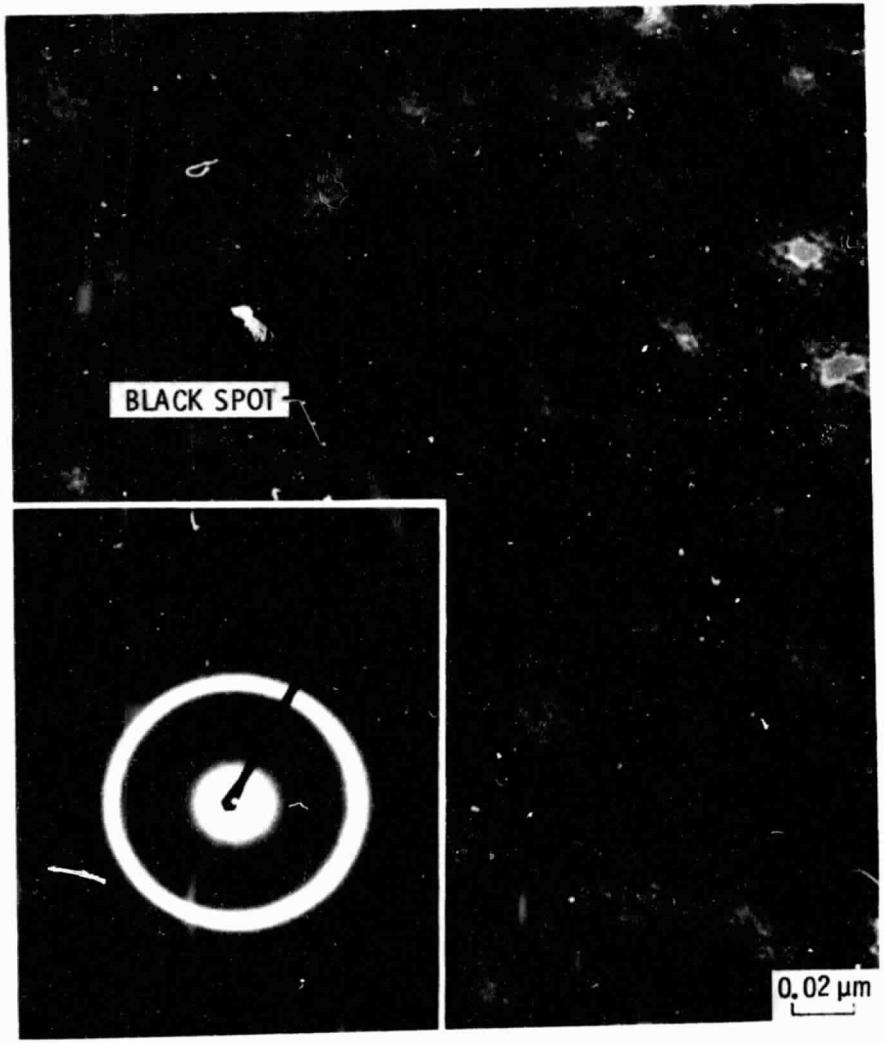

Figure 3. - Typical microstructure and electron diffraction pattern of an amorphous alloy ($Fe_{67}Co_{18}B_{14}Si_1$).

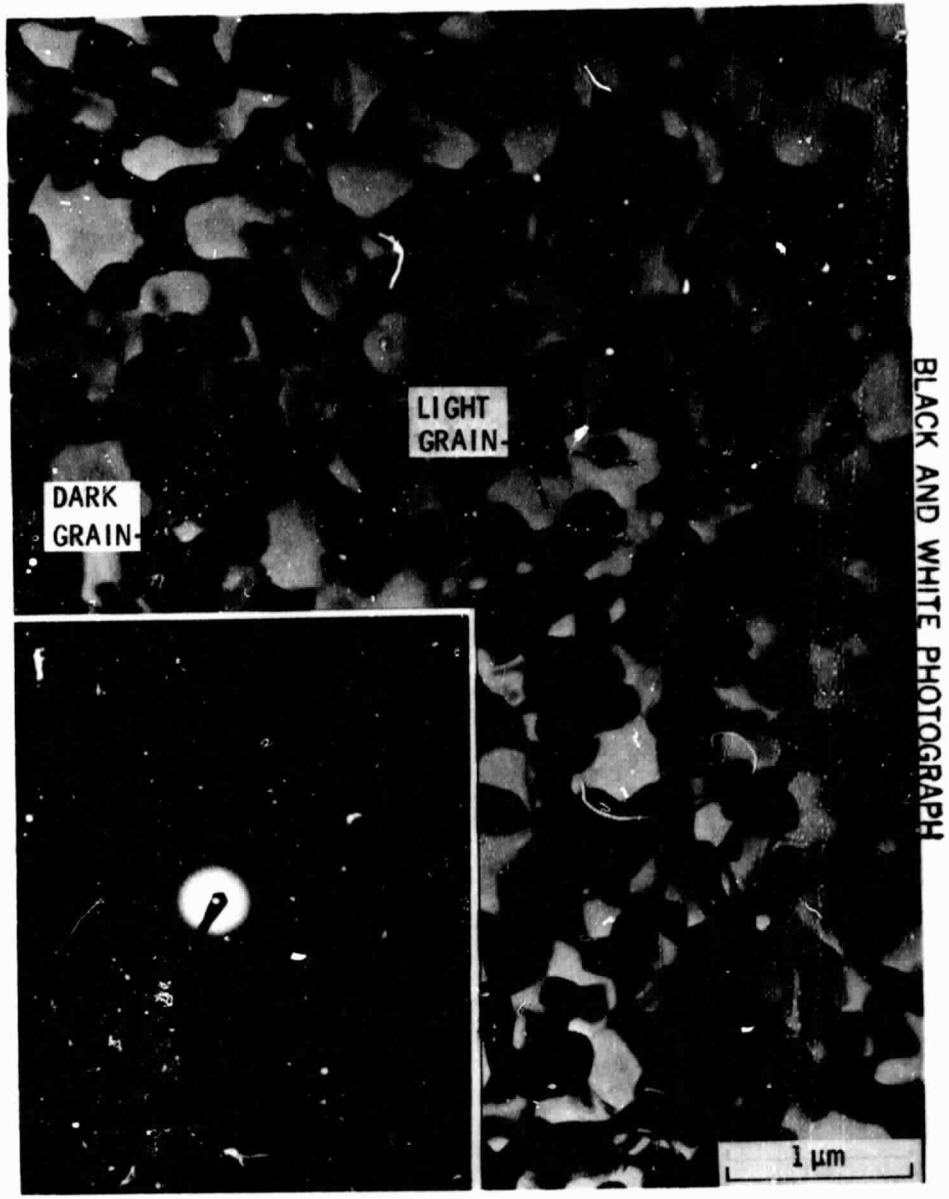

Figure 4. - Typical microstructure and diffraction pattern of an amorphous alloy ($Fe_{67}Co_{18}B_{14}Si_1$) heated to 500° C in vacuum (10 nPa).

ORIGINAL PAGE
BLACK AND WHITE PHOTOGRAPH

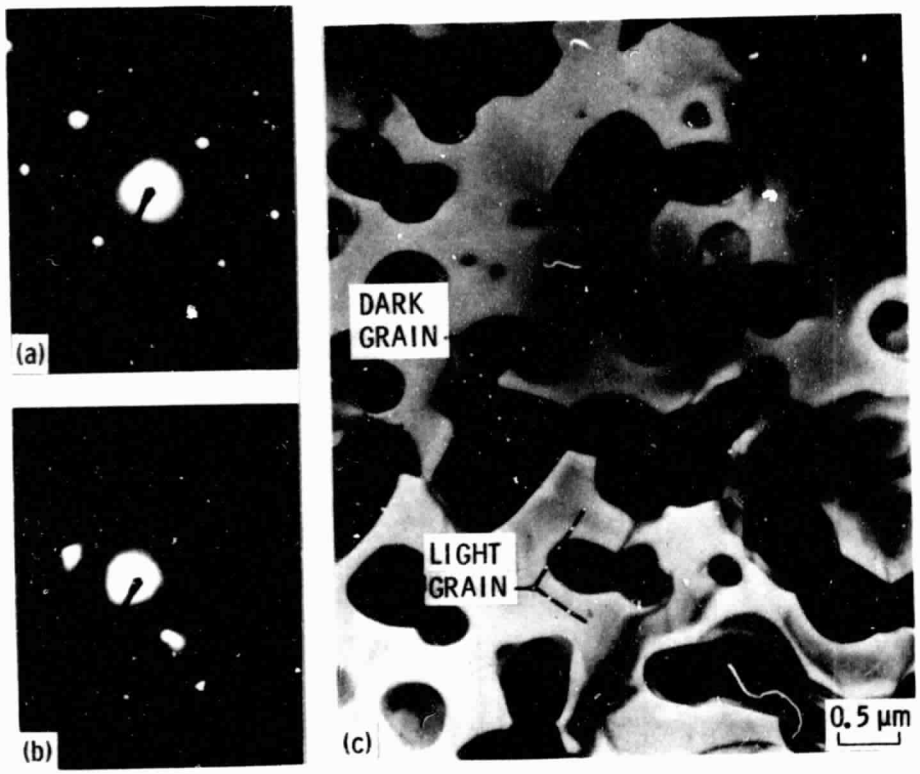

(a) LIGHT GRAIN.

(b) DARK GRAIN.

(c) MICROSTRUCTURE.

Figure 5. - Microstructure and electron diffraction pattern of an amorphous alloy ($Fe_{67}Co_{18}B_{14}Si_1$) heated to 750° C in vacuum (10 nPa).

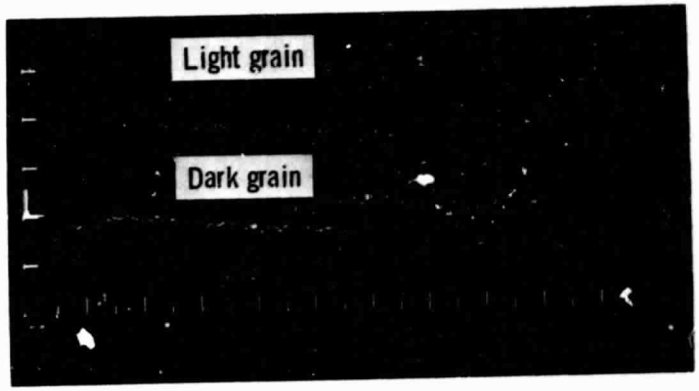

Figure 6. - Energy-dispersive X-ray profile of a metallic glass ($Fe_{67}Co_{18}B_{14}Si_1$) heated to 750° C in vacuum (10 nPa).

ORIGINAL PAGE
BLACK AND WHITE PHOTOGRAPH

ORIGINAL PAGE
BLACK AND WHITE PHOTOGRAPH

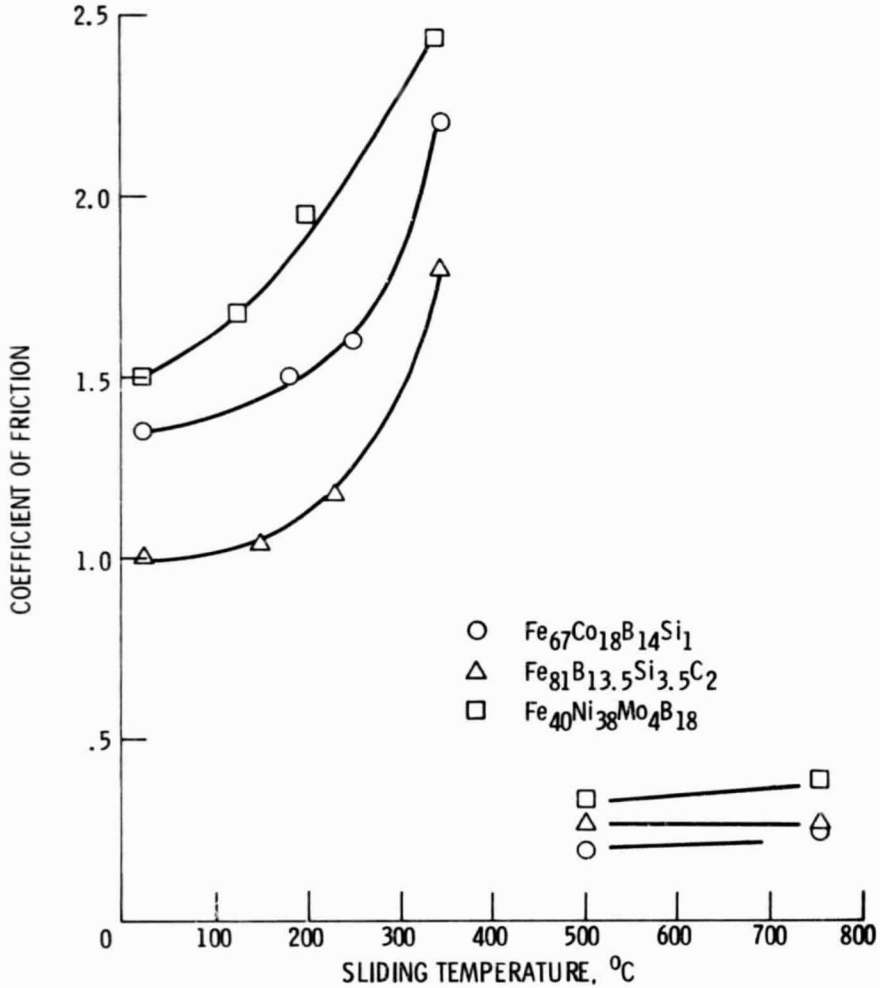

Figure 7. - Coefficient of friction as a function of temperature for aluminum oxide sliding on $Fe_{67}Co_{18}B_{14}Si_1$, $Fe_{81}B_{13.5}Si_{3.5}C_2$, and $Fe_{40}Ni_{38}Mo_4B_{18}$ in vacuum. Normal load, 0.2 N; sliding velocity, 3 mm/min; vacuum, 10 nPa.

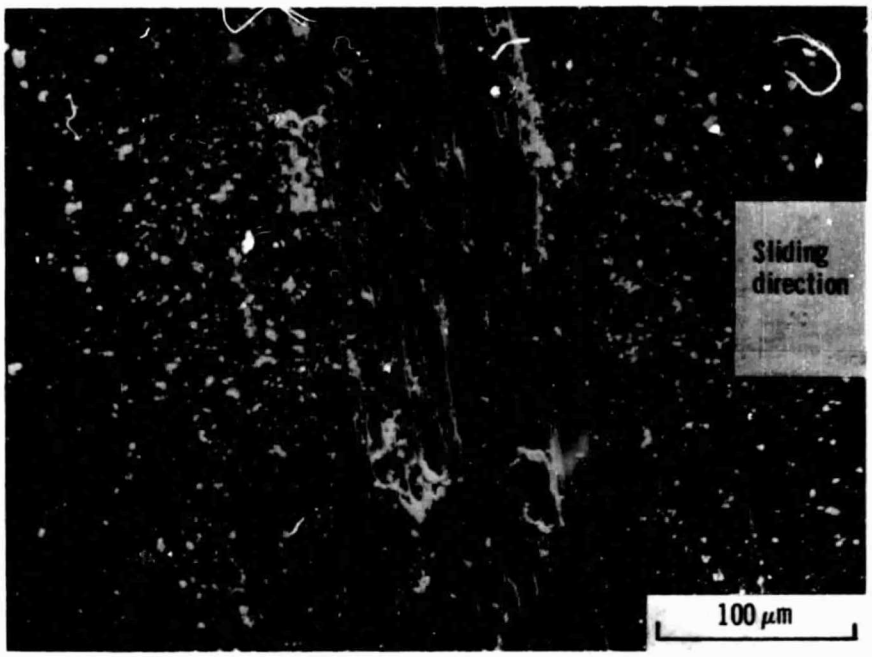

Figure 8. - Scanning electron micrograph of 304 stainless steel wear surface. Pin, 6.4 millimeters diameter aluminum oxide sphere; load, 2.5 newtons; dry sliding in an argon atmosphere; sliding velocity, 0.3 millimeters per second; room temperature.

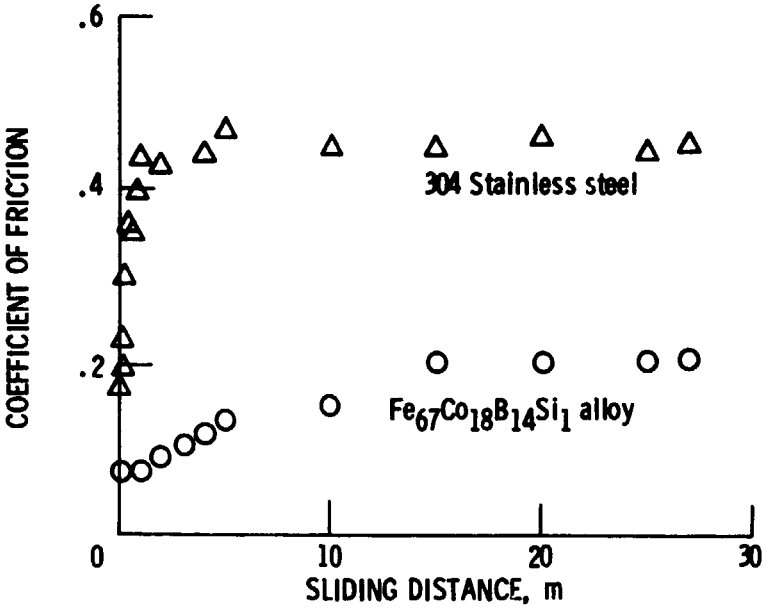

Figure 9. - Coefficient of friction as a function of sliding time for Fe_{67} Co_{18} B_{14} Si_1 amorphous alloy and 304 stainless steel in a laboratory air atmosphere. Pin, 3.2 mm diameter aluminum oxide sphere; load, 2.5 N; sliding velocity, 1.5 mm/sec; room temperature; relative humidity, 40%.

ORIGINAL PAGE
BLACK AND WHITE PHOTOGRAPH

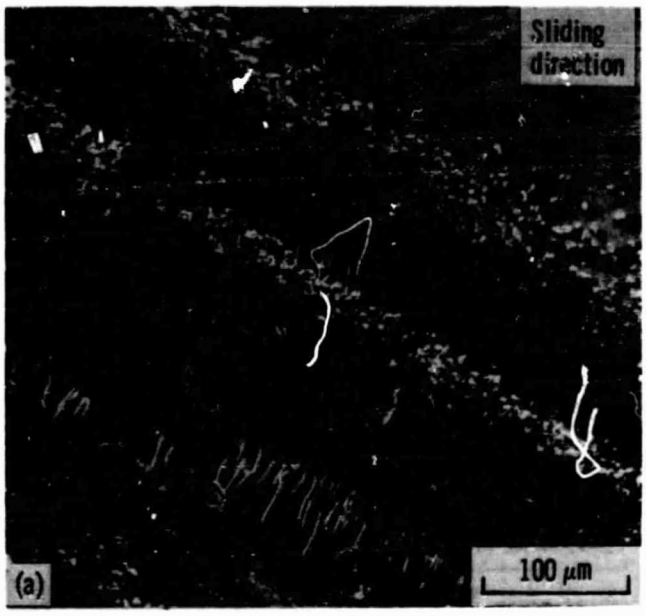

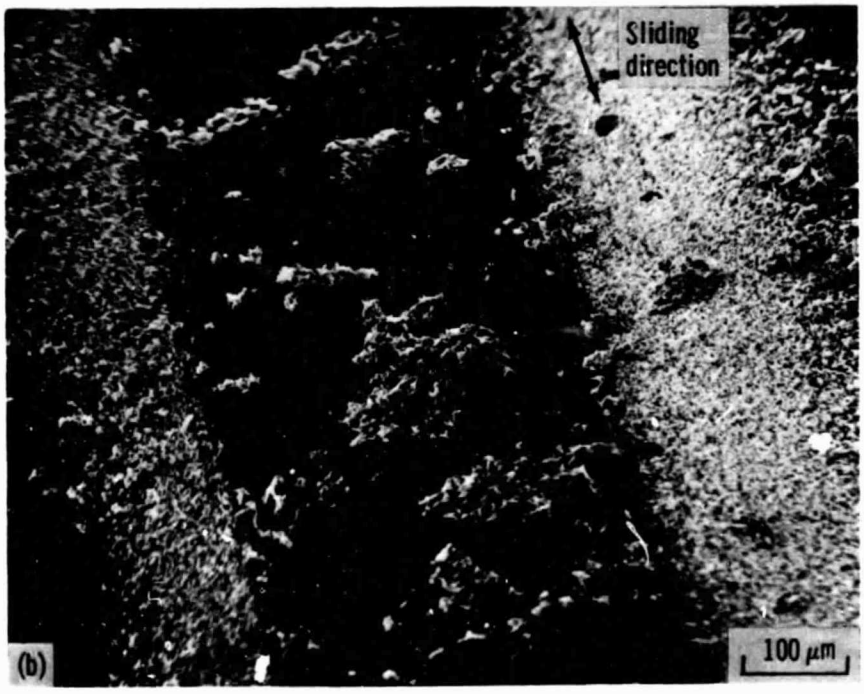

(a) $Fe_{67}Co_{18}B_{14}Si_1$.

(b) 304 stainless steel.

Figure 10. - Scanning electron micrographs of wear track on $Fe_{67}Co_{18}B_{14}Si_1$ amorphous alloy and wear track on 304 stainless steel. Pin, 3.2 millimeters diameter aluminum oxide sphere; load, 2.5 newtons; sliding velocity, 1.5 millimeters per second; sliding distance, 27 meters; room temperature; laboratory air atmosphere; relative humidity, 40%.

ORIGINAL PAGE
BLACK AND WHITE PHOTOGRAPH

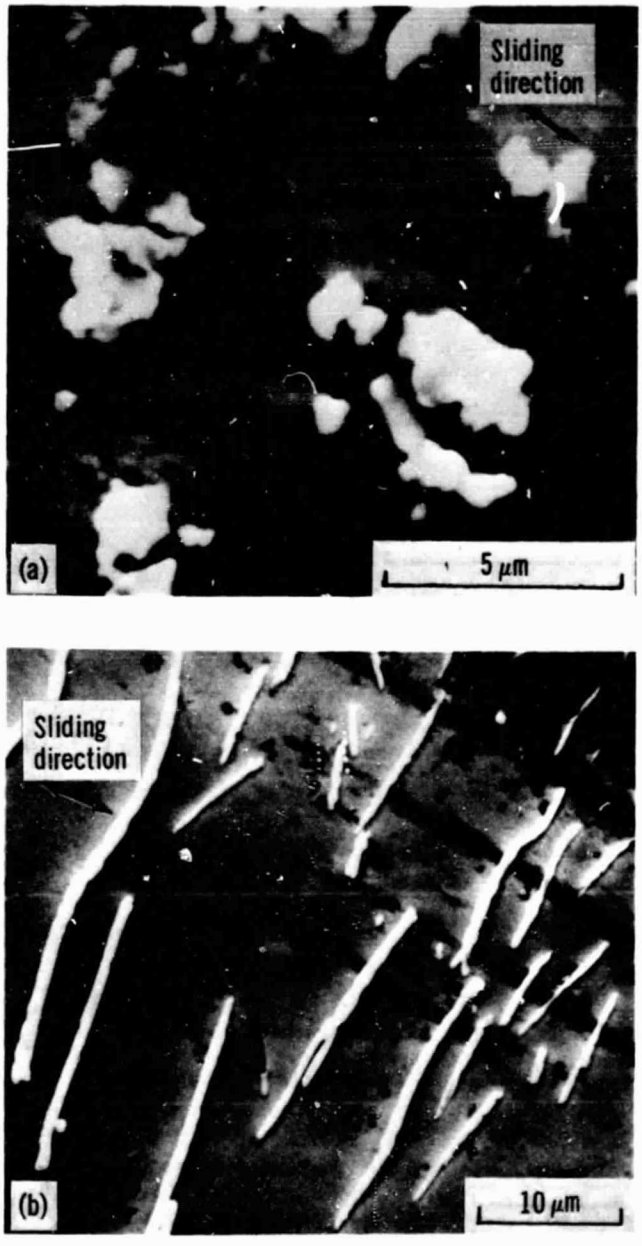

(a) Powdery debris.

(b) Whiskery debris.

Figure 11. - Scanning electron micrographs of powdery and whiskery wear debris particles produced on $Fe_{67}Co_{18}B_{14}Si_1$ amorphous alloy. Pin, 3.2 millimeters diameter aluminum oxide sphere; sliding velocity, 1.5 millimeters per second; load, 2.5 newtons; sliding distance, 27 meters; room temperature; laboratory air atmosphere; relative humidity, 40%.

ORIGINAL PAGE
BLACK AND WHITE PHOTOGRAPH

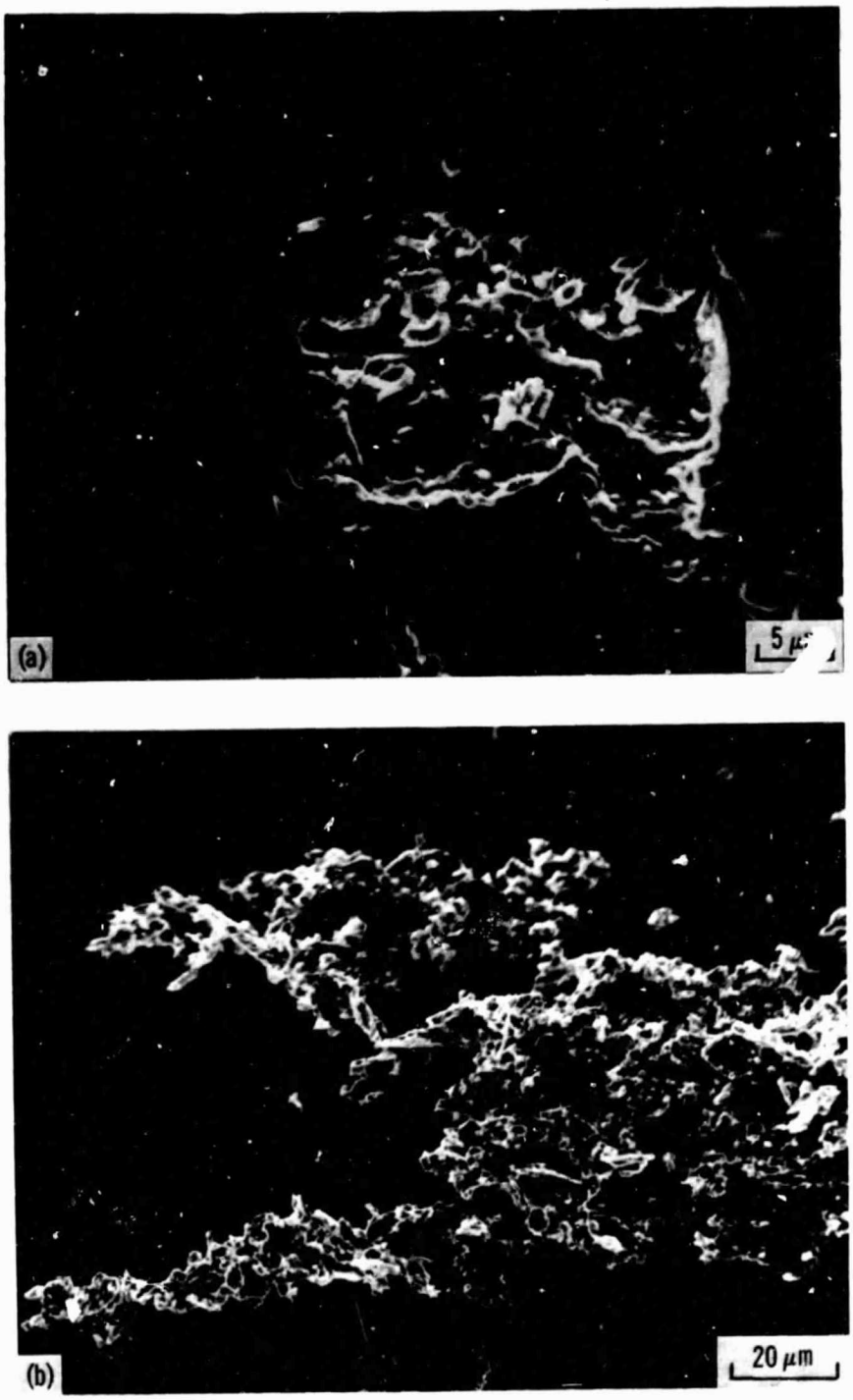

(a) Cavity.

(b) Wear debris.

Figure 12. - Scanning electron micrographs of wear track on 304 stainless steel. Pin, 3.2 millimeters diameter aluminum oxide sphere; load, 2.5 newtons; sliding velocity, 1.5 millimeters per second; sliding distance, 27 meters; room temperature; laboratory air atmosphere; relative humidity, 40%.